Evanescent wave amplification and subwavelength imaging by ultrathin uniaxial μ-near-zero material

Yan Zhao[a]
International School of Engineering, Faculty of Engineering, Chulalongkorn University, Bangkok 10330, Thailand

(Received 19 August 2013; accepted 10 February 2014; published online 18 February 2014)

We demonstrate strong evanescent wave amplification by a thin slab of uniaxial μ-near-zero (UMNZ) material. It is found that while retaining the same amplification effect, the slab can be made arbitrarily thin when the negative permeability along the axis of anisotropy approaches zero. Numerical results show that using a single layer of split-ring resonators (SRRs) with its thickness equal three thousandth of the incident wavelength ($\lambda/3000$), a subwavelength source distribution with $\lambda/4$ resolution can be transferred to a distance of $\lambda/3$. [http://dx.doi.org/10.1063/1.4866579]

In 2000, Pendry proposed a concept of 'perfect lens',[1] which is formed by the so-called left-handed material (LHM) with simultaneously negative permittivity and permeability.[2] The perfect lens requires ideal material parameters, and is physically unrealizable due to the inherent material loss in reality. Despite this fact, a considerable amount of effort has been made on the realization of superlenses.[3–5] Their operations rely on the amplification of evanescent waves to restore fine details of a source, thus subwavelength imaging with resolution below the diffraction limit can be achieved.[1]

Recently, there is a growing interest in the design of thin metamaterial structures. Their low profile may enable the realization of many novel devices such as ultrathin absorbers,[6–8] polarization-changing devices,[9,10] ultralow profile cloaks,[11,12] and thin Luneburg lens[13,14] etc. In the current work, we investigate the possibility of constructing planar superlenses using ultrathin uniaxial metamaterials. It is found from our analysis that the superlens can be made arbitrarily thin when the negative material parameter along the axis of anisotropy approaches zero, while nearly the same amplification effect of evanescent waves can be retained.

In literature the ϵ-near-zero (ENZ) and μ-near-zero (MNZ) materials have been extensively studied to explore their potential applications such as shaping the radiation pattern of antennas,[15] improving transmission through waveguide bends,[16] enhancing wave absorption,[8] as well as subwavelength imaging.[17,18] However, the thickness of the considered structures[17,18] is electrically large, and two components of the permittivity or permeability tensor need to be controlled simultaneously. As it will be shown in this letter, only a single component of the permeability tensor along the axis of anisotropy needs to be determined for subwavelength imaging, which may significantly ease the implementation of the proposed superlens structure.

Here we consider an electrically thin slab of uniaxial MNZ (UMNZ) material with its permittivity and permeability tensor specified as

$$\varepsilon = \varepsilon_0, \quad \boldsymbol{\mu} = \mu_0 \begin{pmatrix} 1 & 0 & 0 \\ 0 & \mu_y & 0 \\ 0 & 0 & 1 \end{pmatrix}. \tag{1}$$

[a]yan.z@chula.ac.th

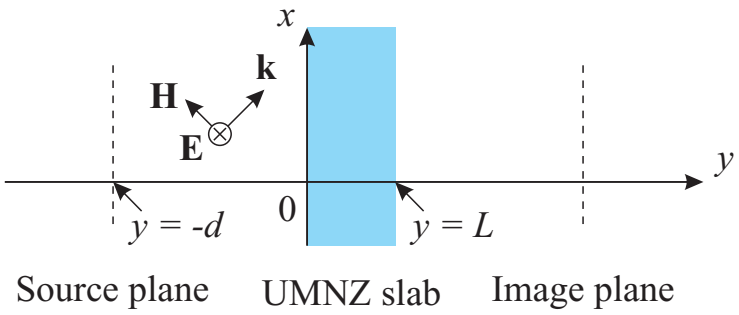

FIG. 1. System configuration for the analysis of plane-wave transmission through a UMNZ slab.

The slab is infinite along x- and z-directions, thus it interacts strongly with transverse electric (TE) polarized waves (with respect to the slab interface), with only three non-zero field components H_x, H_y, and E_z. The system configuration is shown in Fig. 1, with the UMNZ slab placed between $y = 0$ and $y = L$. The source plane is located at $y = -d$, and the location at a certain distance away behind the slab is regarded as the image plane.

Assuming plane-wave incidence upon the UMNZ slab, the tangential electric and magnetic field components E_z and H_x in different regions can be expressed as

$$E_z = E_0 e^{-jk_x x} \begin{cases} e^{-jk_y y} + Re^{jk_y y}, & y < 0, \\ Ae^{-j\kappa_y y} + Be^{j\kappa_y y}, & 0 \le y \le L, \\ Te^{-jk_y (y-L)}, & y > L, \end{cases} \tag{2}$$

$$H_x = \frac{E_0 e^{-jk_x x}}{\omega\mu_0} \begin{cases} k_y (e^{-jk_y y} - Re^{jk_y y}), & y < 0, \\ \kappa_y (Ae^{-j\kappa_y y} - Be^{j\kappa_y y}), & 0 \le y \le L, \\ k_y Te^{-jk_y (y-L)}, & y > L, \end{cases} \tag{3}$$

where E_0 is the magnitude of the incident wave, k_x and k_y are wave numbers along x- and y-directions in freespace, respectively ($k_x^2 + k_y^2 = k_0^2$ where k_0 is the freespace wave number), κ_y is the wave number along y-direction inside the UMNZ slab, R and T are reflection and transmission coefficients, and A and B are the amplitudes of waves inside the slab traveling in forward and backward directions, respectively. By matching boundary conditions at $y = 0$ and $y = L$ such that the tangential field components (1) and (2) are continuous, the transmission coefficient from the front to the back interfaces of the UMNZ slab can be calculated as

$$T = \frac{2\kappa_y k_y}{(\kappa_y + k_y)^2 e^{-j\kappa_y L} - (\kappa_y - k_y)^2 e^{j\kappa_y L}}, \tag{4}$$

and the total transmission coefficient from the source to the image planes can be expressed as

$$T' = \frac{2\kappa_y k_y e^{-jk_y (y+d-L)}}{(\kappa_y + k_y)^2 e^{-j\kappa_y L} - (\kappa_y - k_y)^2 e^{j\kappa_y L}}, \tag{5}$$

where κ_y can be calculated from the dispersion relation for the UMNZ slab:

$$\frac{k_x^2}{\mu_y} + \kappa_y^2 = k_0^2. \tag{6}$$

It is well known that surface plasmon-like modes can be excited at the interface between media with positive and negative material parameters. For a layered structure with negative material parameters embedded in a medium with positive ones, strong resonant modes can be supported.[19] The resonant conditions for such modes are given by the solutions to the following equation:

$$(\kappa_y + k_y)^2 e^{-j\kappa_y L} = (\kappa_y - k_y)^2 e^{j\kappa_y L}, \tag{7}$$

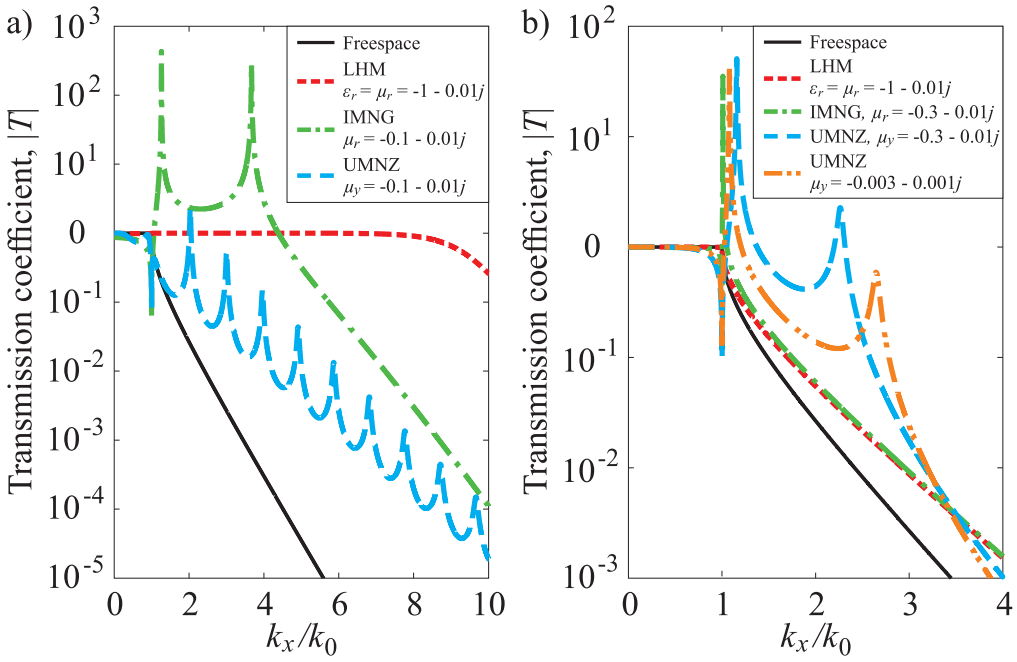

FIG. 2. Transmission coefficients for (a) thick slabs with $L = 5$ mm, and (b) thin slabs with $L = 1$ mm (LHM, IMNG and UMNZ (cyan, long dashed line)) and $L = 0.01$ mm (UMNZ (orange, dot-dashed line)). The incident wavelength is 30 mm, and the distance between the source and image planes is 10 mm. A small amount of loss is added to all materials.

i.e. when the denominator of Eq. (4) equals zero. Equation (7) cannot be solved by any direct means, but its solutions may be expressible using the so-called Lambert W function,[20] or approximated using the Newton's method. Alternatively, we evaluate the transmission coefficients given by Eq. (5) with varying transverse wave numbers k_x, to analyze the resonances and amplification effects of evanescent waves.

Figure 2 shows the calculated transmission coefficients for different thicknesses of the UMNZ slab. For comparison, the transmission coefficients through slabs formed by LHM and isotropic μ-negative material (IMNG) are also shown. For these two types of material, Eq. (5) remains valid, while κ_y can be calculated from the dispersion relation: $k_x^2 + \kappa_y^2 = \varepsilon_r \mu_r k_0^2$, where $\varepsilon_r = \mu_r = -1$ for LHM and $\varepsilon_r = 1$, $\mu_r < 0$ for IMNG. From Fig. 2, it is apparent that when the thickness is large, LHM and IMNG slabs offer greater enhancement of evanescent waves and better subwavelength imaging capability. In addition, while no resonance is found for the LHM slab due to its matched impedance, and two resonances are identified for the IMNG slab, multiple resonances can be observed for the UMNZ slab. This is due to the fact that the introduced anisotropy of the material creates additional resonant conditions, as it can be analyzed from Eqs. (5) and (6). The locations of these resonances are sensitive to the slab thickness and material parameters. When the thickness is small, the resonances (except the fundamental one) shift to larger wave numbers. In particular, when the thickness is less than one-tenth of the distance between the source and image planes, the amplification effect reduces to its minimum for the IMNG and LHM slabs, as illustrated by Fig. 2(b). While for UMNZ, there still exists a second resonance at a small wave number, which can be shifted even lower when μ_y is increased but remains negative, such that the amplification effect can be retained when the slab thickness is further reduced. A remarkable result is that when $\mu_y \to 0^-$, the thickness of the UMNZ slab can be made arbitrarily small. A comparison of transmission coefficients for two UMNZ slabs with their thicknesses equal $\lambda/30$ and $\lambda/3000$ shows a similar amplification effect, while the thickness of the latter slab is one hundred times smaller. This enables the construction of extremely thin superlenses using the UMNZ material.

To demonstrate the subwavelength imaging capability of the UMNZ superlens, we perform full-wave finite element simulations and model two UMNZ slabs with their thicknesses equal $L = 1$

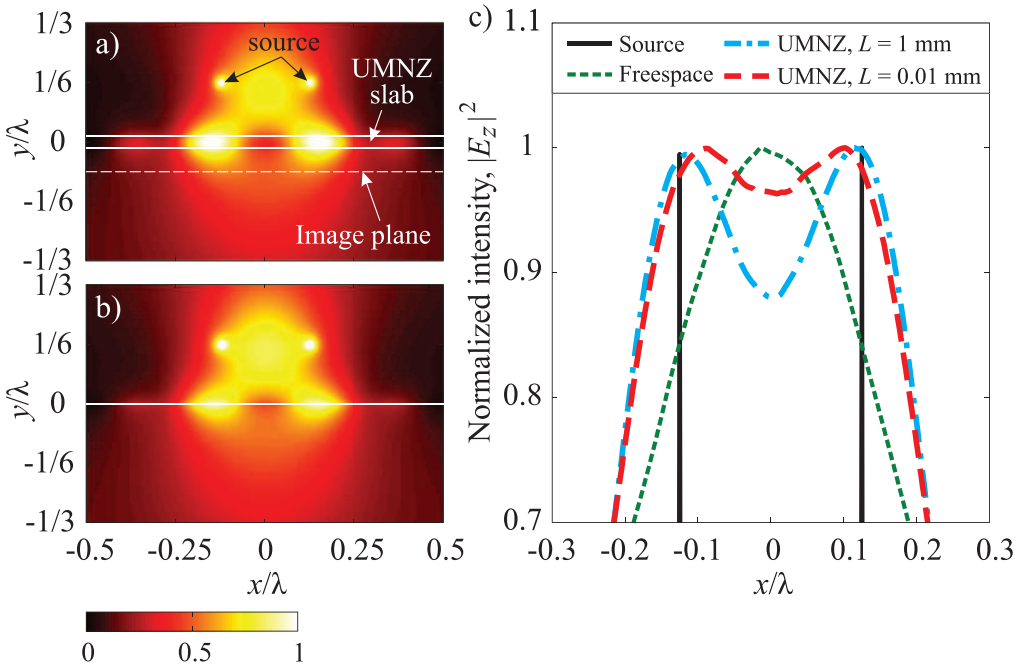

FIG. 3. Normalized distributions of electric field intensity calculated from simulations of subwavelength imaging using thin UMNZ slabs with (a) $L = 1$ mm, $\mu_y = -0.35 - 0.01j$, and (b) $L = 0.01$ mm, $\mu_y = -0.0031 - 0.001j$. (c) Normalized electric field intensity in x-direction at 7.5 mm (λ/4) away from the source plane.

mm (λ/30) and $L = 0.01$ mm (λ/3000). The operating frequency is 10 GHz. The transverse dimension of the slabs is 30 mm (λ) in x-direction. The perfect electric conductor (PEC) boundary condition is applied to z-direction for modeling infinite UMNZ slabs. Two in-phase electric line sources oriented in z-direction are excited at 5 mm (λ/6) away from the front interface of the slabs, and the distance between the sources is 7.5 mm (λ/4). The overall dimensions of the simulation domain are $60 \times 40 \times 0.3$ mm^3. The calculated distributions of electric field intensity in the central region of the x-y plane are shown in Figs. 3(a) and 3(b), when images with the highest subwavelength resolutions are obtained (by varying μ_y). It can be seen that for both cases, strong plasmonic resonances are excited at the interfaces of the slabs, and subwavelength details of the source are coupled to a significant distance away beyond the slab. The electric field intensity in the image plane located at 7.5 mm (λ/4) away from the sources are plotted in Fig. 3(c), and show that the two maxima with λ/4 apart are clearly resolved. The better subwavelength imaging performance of the thicker slab is due to the excited stronger plasmonic resonance.

For the implementation of the UMNZ slab, we consider a planar structure formed by capacitively loaded split-ring resonators (SRRs). The unit cell of the structure is shown in Fig. 4(a). A plane-wave analysis is performed to retrieve the effective permeability of the structure.[21] The extracted relative permeability for the single-layer SRR structure is shown in Fig. 4(b). Note that the simulated structure for permeability retrieval is periodic along both y- and z-directions;[21] while the structure for subwavelength imaging is only infinite in z-direction, and finite along x-direction with its transverse dimension equal 30 mm (λ). Thus the extracted permeability only provides a guidance for tuning the SRR structure, and the dimension of the unit cell should be sufficiently small comparing with the wavelength. The intensity distribution when an image with the highest resolution is obtained (by varying the capacitance) is shown in Fig. 4(c), similar to the distribution in Fig. 3(b). In addition, a sharper subwavelength image is obtained for the single-layer SRR structure, which may be due to the fact that the actual loss of the structure is smaller. At a distance of λ/3 from the source plane, two maxima are still clearly visible. The transverse dimension of the lens is also varied in simulations, and no notable variations of the image quality have been observed.

In conclusion, we have demonstrated the amplification of evanescent waves by electrically thin UMNZ slabs, and found that the amplification effect can be retained regardless of the slab

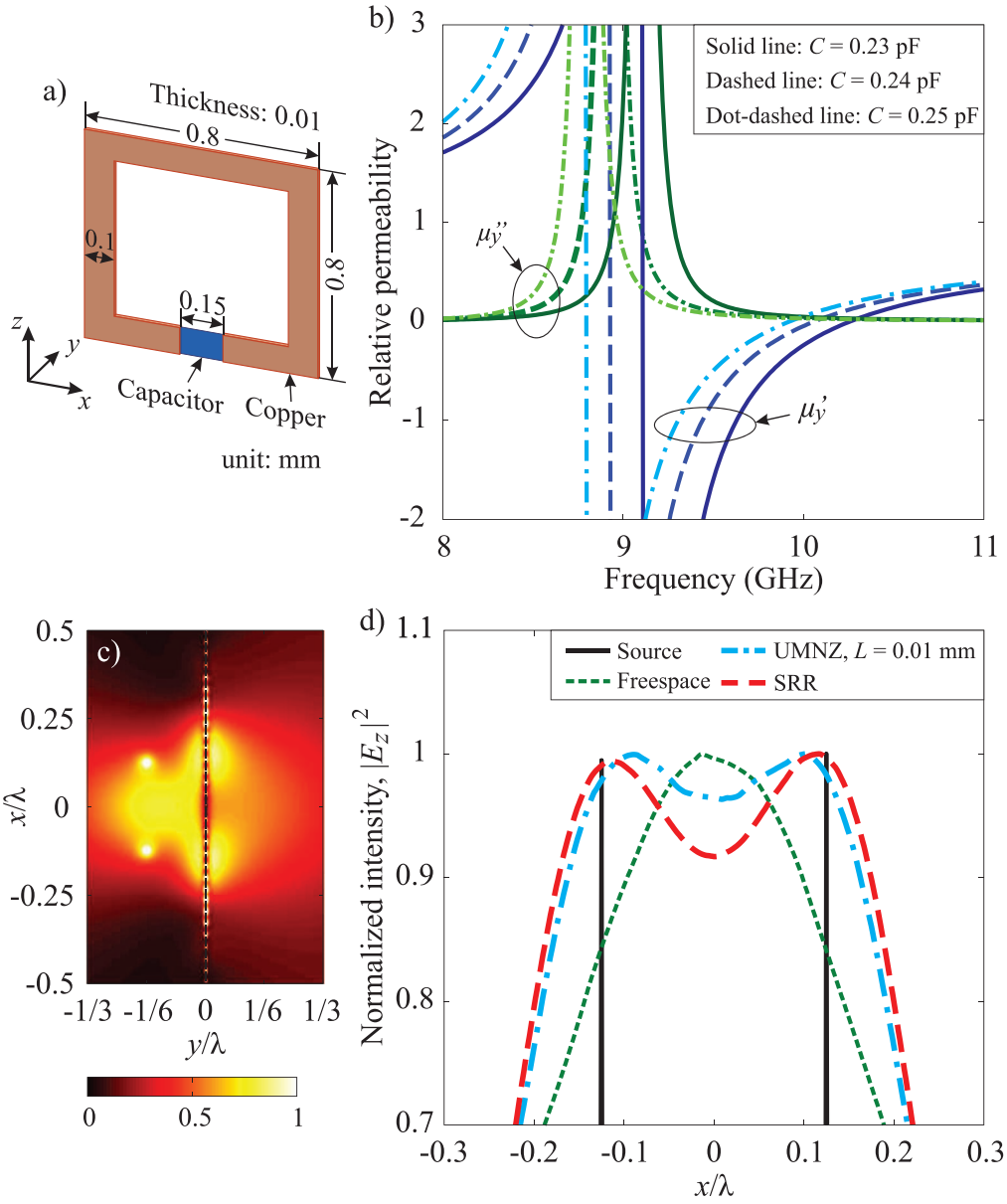

FIG. 4. (a) Unit cell of the single-layer SRR structure. (b) Extracted relative permeability of the capacitively loaded SRR structure. (c) Normalized distribution of electric field intensity calculated from simulations of subwavelength imaging using a single-layer SRR structure ($C = 0.22$ pF). (d) Normalized electric field intensity in x-direction at 7.5 mm ($\lambda/4$) away from the source plane.

thickness, when the permeability along the anisotropy axis is properly chosen. Numerical simulations of a $\lambda/3000$-thick single-layer capacitively loaded SRR structure show that a subwavelength source distribution with $\lambda/4$ resolution can be transferred to a distance of $\lambda/3$. For the practical implementation of the UMNZ superlens, the optimum material parameter can be obtained by analyzing the transmission coefficient and then through an optimization process. It is expected that the proposed structure may find its applications in improving imaging and wireless power transfer systems.

Y. Zhao acknowledges the financial support by The Thailand Research Fund (TRF) Ref. MRG5580226.

[1] J. Pendry, Phys. Rev. Lett. **85**, 3966 (2000).
[2] V. G. Veselago, Sov. Phys. Usp. **10**, 509 (1968).
[3] N. Fang, H. Lee, C. Sun, and X. Zhang, Science **308**, 534 (2005).
[4] T. Taubner, D. Korobkin, Y. Urzhumov, G. Shvets, and R. Hillenbrand, Science **313**, 1594 (2006).
[5] I. I. Smolyaninov, Y.-J. Hung, and C. C. Davis, Science **315**, 1699 (2007).
[6] A. Yanai, M. Orenstein, and U. Levy, Opt. Express **20**, 3693 (2012).
[7] X.-Y. Peng, B. Wang, S. Lai, D. H. Zhang, and J.-H. Teng, Opt. Express **20**, 27756 (2012).
[8] S. Zhong and S. He, Scientific Reports **3**, 2083 (2013).
[9] W. Sun, Q. He, J. Hao, and L. Zhou, Opt. Lett. **36**, 927 (2011).
[10] N. K. Grady, J. E. Heyes, D. R. Chowdhury, Y. Zeng, M. T. Reiten, A. K. Azad, A. J. Taylor, D. A. R. Dalvit, and H.-T. Chen, Science **14**, 1304 (2013).
[11] J. C. Soric, P. Y. Chen, A. Kerkhoff, D. Rainwater, K. Melin, and A. Alu, New J. Phys. **15**, 033037 (2013).
[12] W. X. Jiang, C. Y. Luo, Z. L. Mei, and T. J. Cui, Appl. Phys. Lett. **102**, 014102 (2013).
[13] H. Gao, B. Zhang, S. G. Johnson, and G. Barbastathis, Opt. Express **20**, 1617 (2012).
[14] J. A. Dockrey, M. J. Lockyear, S. J. Berry, S. A. R. Horsley, J. R. Sambles, and A. P. Hibbins, Phys. Rev. B **87**, 125137 (2013).
[15] A. Alu, M. G. Silveirinha, A. Salandrino, and N. Engheta, Phys. Rev. B **75**, 155410 (2007).
[16] B. Edwards, A. Alu, M. E. Young, M. Silveirinha, and N. Engheta, Phys. Rev. Lett. **100**, 033903 (2008).
[17] H. Liu, Shivanand, and K. J. Webb, Opt. Lett. **33**, 2568 (2008).
[18] G. Castaldi, S. Savoia, V. Galdi, A. Alu, and N. Engheta, Phys. Rev. B **86**, 115123 (2012).
[19] A. I. Smolyakov, E. Fourkal, S. I. Krasheninnikov, and N. Sternberg, Prog. Electromagn. Res. **107**, 293 (2010).
[20] R. M. Corless, G. H. Gonnet, D. E. G. Hare, D. J. Jeffrey, and D. E. Knuth, Adv. Comput. Math. **5**, 329 (1996).
[21] D. R. Smith, S. Schultz, P. Markos, and C. M. Soukoulis, Phys. Rev. B. **65**, 195104 (2002).